Inland water bodies in China: Features discovered in the long-term satellite data

Shuailong Feng[a,b], Shuguang Liu[a,b,1], Zhihong Huang[a,b], Lei Jing[a,b], Meifang Zhao[a,b], Xi Peng[a,b], Wende Yan[a,b], Yiping Wu[c], Yihe Lv[d], Andrew R. Smith[e], Morag A. McDonald[e], Sopan D. Patil[e], Arbi J. Sarkissian[e], Zhihua Shi[f], Jun Xia[g], and U. S. Ogbodo[a,b]

[a]National Engineering Laboratory for Applied Technology of Forestry & Ecology in Southern China, Central South University of Forestry and Technology, 410004 Changsha, China; [b]College of Biological Science and Technology, Central South University of Forestry and Technology, 410004 Changsha, China; [c]Department of Earth and Environmental Science, School of Human Settlements and Civil Engineering, Xi'an Jiaotong University, 710049 Xi'an, China; [d]State Key Laboratory of Urban and Regional Ecology, Research Center for Eco-Environmental Sciences, Chinese Academy of Sciences, 100085 Beijing, China; [e]School of Natural Sciences, Bangor University, LL57 2UW Gwynedd, United Kingdom; [f]College of Resources and Environment, Huazhong Agricultural University, 430070 Wuhan, China; and [g]State Key Laboratory of Water Resources and Hydropower Engineering Science, Wuhan University, 430072 Wuhan, China

Edited by Gregory P. Asner, Arizona State University, Tempe, AZ, and approved November 3, 2019 (received for review June 25, 2019)

Water bodies (WBs), such as lakes, ponds, and impoundments, provide essential ecosystem services for human society, yet their characteristics and changes over large areas remain elusive. Here we used unprecedented data layers derived from all Landsat images available between 1984 and 2015 to understand the overall characteristics and changes of WBs between 2 epochs (i.e., 1984 to 1999 and 2000 to 2015) in China. Results show that the abundance estimate of WBs greater than 1 km^2 and the total WB surface area were 0.3 to 1.5 times and 0.2 to 0.5 times more than the previous estimates, respectively. The size-abundance and shoreline-area relationships of WBs in China conformed to the classic power scaling law, in contradiction to most previous studies. WB changes with various occurrence probabilities show widespread coexistence of disappearance of existent and emergence of new WBs across China driven primarily by human activities and climate change. Our results highlight the importance of using appropriate long-term satellite data to reveal the true properties and dynamics of WBs over large areas, which is essential for developing scaling theories and understanding the relative impacts of human activities and climate change on water resources in the world.

inland water bodies | size-abundance | land use change | climate change

The provisioning of freshwater is an essential ecosystem service for humankind, and such services include water supply, biomass and food production regulation, communication and transportation, wildlife habitats, biogeochemical cycles, and climate regulation (1–3). Fresh water bodies (WBs) are under constant change because of the impacts of anthropogenic activities and climate change (4). Monitoring the dynamic changes of WBs and understanding their causes and consequences have important implications to the resilience of social-ecological systems (5, 6).

The abundance and area of WBs over large regions are critical information for water-resource management but remain highly elusive. For example, the number of lakes larger than 0.1 km^2 at the global scale was estimated to range from 246,146 to 4,123,551 (7, 8), more than 1 order of magnitude difference among them. The estimated area of lakes larger than 0.1 km^2 varied from 2,428,100 km^2 to 4,080,000 km^2 respectively, and the largest difference was 68%. These huge differences among various studies call for innovative investigations to reduce the uncertainties in the number and area of WBs.

Biogeochemical processes in WBs represent major components in the cycle of carbon, nutrients, and other materials at the regional to global scales (9, 10). Estimating biogeochemical processes such as greenhouse gas fluxes from WBs from regional to global scales has been challenging because these processes are size dependent (11). Finding the size-abundance relationship therefore has been a persistent effort for over a century to facilitate the scaling of heterogeneous processes across various WBs (12). Although a power law relationship has been reported in many studies, deviations exist, particularly for small WBs (8, 13–15) and in mountainous regions (16) where topographic relief, geology, and complexity of landscapes are thought to affect the goodness of fit to the power scaling law (14). The existence of the power law and its dependence on topography and geology needs to be evaluated more extensively.

Water-resource management and planning as well as climate change adaptation rely heavily on the knowledge of long-term trends and spatial dynamics of surface WBs (1). However, progress on characterizing the dynamics of WBs over large regions has been hindered by data availability, dynamic nature of WBs, complexity of driving forces, and geospatial heterogeneity of environments (8). Most previous studies do not have enough data points in time to capture the temporal changes of WBs, and consequently the overall dynamics and size dimensions of the WBs, particularly the intermittent WBs, are not well represented (17, 18). Recently, an unprecedented effort by Pekel et al. (19) has generated a global surface water dataset that describes the changes

Significance

Inland water bodies (WBs) provide essential ecosystem services for human society, yet their characteristics and changes over large areas remain elusive. We used unprecedented data layers derived from Landsat imagery to quantify and decipher the spatial distributions and contemporary changes of WBs in China. The results shed light on the characteristics (e.g., abundance and size-abundance and shoreline-area relationships) and spatiotemporal dynamics of WBs. This study highlights the importance of using appropriate long-term satellite data to reveal the true properties and dynamics of WBs over large areas, which is essential for developing theories and understanding the predominant impacts of human activities and climate change on water resources not only in China but also in other regions of the world.

Author contributions: S.F. and S.L. designed research; S.F., S.L., Z.H., and Y.L. performed research; S.F. contributed new reagents/analytic tools; S.F., S.L., L.J., M.Z., W.Y., Y.W., A.J.S., Z.S., and U.S.O. analyzed data; and S.F., S.L., X.P., A.R.S., M.A.M., S.D.P., and J.X. wrote the paper.

The authors declare no competing interest.

This article is a PNAS Direct Submission.

Data deposition: All data used in support of this manuscript are available in Figshare, https://figshare.com/s/9e931d6db628e3f96689 (DOI: 10.6084/m9.figshare.9959516).

[1]To whom correspondence may be addressed. Email: shuguang.liu@yahoo.com.

This article contains supporting information online at https://www.pnas.org/lookup/suppl/doi:10.1073/pnas.1910872116/-/DCSupplemental.

First published December 2, 2019.

in WBs from 1984 to 2015 at 30 m resolution. Although the overall global patterns of WB changes have been analyzed, more detailed and elaborate analyses are sorely needed at regional and continental scales to better understand the spatial and temporal patterns of WB changes and to test the validity of existing theories such as the controversial power scaling law for the size-abundance relationship (12, 20, 21). China represents an ideal place for such as study because of its vast heterogeneous territories, intensified human activities in recent decades, and large uncertainties in the characterization of its dynamic water resources (22).

Abundance, Area, and Scaling of WBs

Our estimate of WB abundance in China exceeds all previous estimates (*SI Appendix*, Tables S1 and S2). The abundance of WBs (>1 km^2) is estimated to be 6,821 in our study, 1.3 times the previous highest estimate (5,535) and 2.5 times the lowest estimate (2,693) (7, 17, 23, 24). The number of WBs larger than 0.0036 km^2 in China is 688,617 in this study, much higher than 275,029 estimated previously (24). Our estimates of WB area in China are higher than those from previous studies. For example, our estimate of total area of WBs larger than 0.0036 km^2 in China is 134,158 km^2, 23% higher than 109,102 km^2 estimated by Yang et al. (24). The total area of WBs larger than 1 km^2 is estimated to be 123,342 km^2 in our study, 22 to 51% larger than the previous estimates (7, 17, 23, 24). Similar differences can be found across the regions in China as well. For example, the number of medium and large WBs in the YTR (Yangtze River basin, acronyms for the river basins are listed in *SI Appendix*, Table S3) is estimated to be 1,952 in this study, much higher than 1,395 estimated by Yang et al. (25). The medium and large WBs in the Tibetan Plateau basin (TP) amount to 1,289 in our study, which is very close to Mao et al. (26) (1,291), but higher than Wan et al. (27) (1,055) and Lu et al. (28) (1,044). We found that the total area of WBs larger than 0.0036 km^2 in the YTR is 36,710.83 km^2, which is 48% higher than Yang et al. (25) (24,842 km^2). Our estimate of the WBs larger than 1 km^2 in the TP is 56,247.41 km^2, much higher than Mao et al. (26) (46,264.5 km^2) or Wan et al. (27) (41,831 km^2).

The overall exceedance of our WB estimates can largely be attributed to the differences in methodology. Conventionally, WBs over large areas are characterized using 1 or a few snapshots of remotely sensed images, which could not consistently capture intermittent WBs and historical maximum water extents (MWEs) (29). Previous results are therefore contingent to the snapshot-specific climate and hydrological conditions at the time that images were taken.

The size-abundance relationships in China conform to the power law with a Pareto coefficient of −0.835 (*SI Appendix*, Fig. S1*F* and Table S4), similar to −0.85 reported for the contiguous United States (CONUS) (30), but higher than that for the world in 2004 (−0.992) (7) and in 2016 (−1.054) (17). At a regional scale, the Pareto coefficient in the TP is −0.662, the highest among all regions, signifying a higher fraction of large WBs in the TP compared to other regions (*SI Appendix*, Table S5). In contrast, the scaling exponent in the Pearl River basin (PR) basin is −0.941, the lowest among all regions, representing a relatively higher share of small lakes. Comparatively, the log-transformed WB size-abundance distribution in China presented a shallower slope or Pareto coefficient than those in the world and CONUS, suggesting that small WBs are relatively more abundant in China than in the CONUS and the world (Fig. 1*C*). Our results show the power scaling law between abundance and size of WBs in China, despite its complex geography and topographic characteristics, is different from a number of recent studies that have found deviations from the power scaling law, particularly for small WBs (8, 13–15). Seekell et al. (13) show that the size-abundance relationship in a mountainous region (Adirondack, USA) did not follow the power scaling law while it fit well in a flat region (Gotland, Sweden), and argue that the topographic relief, geology, and complexity of the

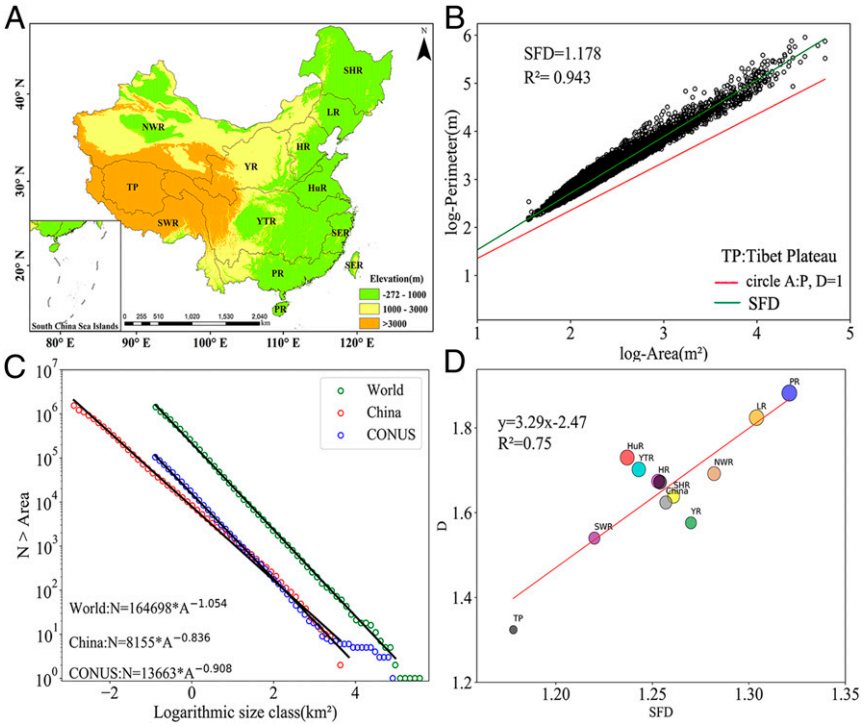

Fig. 1. Boundaries of regions, morphological, and size-abundance scaling of water bodies in China. (*A*) Locations and boundaries of the 11 regions in China; (*B*) SFDs of TP. (*C*) Size-abundance distributions of water bodies in China, CONUS, and the world. (*D*) SFDs and fractal dimension of size-abundance in China and the regions.

landscapes could impact how well data fit the simple power scaling law. It is quite surprising to see that our results fit the power scaling law well in China even though some regions such as the TP, and northwestern and southwestern China are famous for their high topographic relief and steep slopes that are suspected to cause deviations from the power scaling law (Fig. 1*B* and *SI Appendix*, Fig. S2).

The shoreline fractal dimension (SFD) derived from dimensional analysis (log perimeter-log area analysis) is often used to indicate the influences of human modifications or geology on the shape of WBs (31). The SFD ranges from 1.178 in TP to 1.321 in PR (Fig. 1*B* and *SI Appendix*, Fig. S3). Theoretically, the fractal dimension of size-abundance (D) (D = 2 *abs(c), c is the scaling exponent or Pareto coefficient mentioned above) is supposed to be similar to the SFD (13, 32). We compared the D and SFD derived from China and found a strong linear relationship between these 2 fractal dimensions ($D = 3.13 \times SFD - 2.27$, $R^2 = 0.73$, $P < 0.05$). However, the slope is significantly different from 1, suggesting that our results do not support the theoretical equivalency of these 2 fractal dimensions (Fig. 1*D*). The deviation of D and SFD from the theoretical equivalency might be caused by increased frequency of smaller WBs and/or effort in shaping WBs more regularly and reducing the sinuosity of WB boundaries. Economic growth and aquaculture intensification have propelled the increase of smaller WBs and geometric regularization of the WBs, particularly in the southeastern and coastal parts of China (33).

Various Changes between 2 Epochs

Overall changes of WBs in China between the 2 epochs (i.e., 1985 to 1999 and 2000 to 2015) are shown in Fig. 2, which reveals that 53.9% of the WBs remain unchanged nationwide, and further shows the various degrees of change between the epochs. A total of 5,197.09 km^2 or 3.92% of the WB area in China disappeared (absolutely decreased); whereas the very likely (with 75 to 99% probability), likely (with 25 to 74% probability), and unlikely (with 1 to 24% probability) decreases accounted for 1.6%, 6.23%, and 7% of the total WB area, respectively (Fig. 3 and *SI Appendix*, Table S6). A total of 9,040.26 km^2 were converted from nonwater surfaces into WBs (absolutely increased), corresponding to 6.81% of the total WB area in China. At the same time, very likely, likely, and unlikely increase occurred on 3.76%, 8.18%, and 5.71% of the total WB area, respectively. The large WBs (>10 km^2) explain most of the very likely, likely, and unlikely increase or decrease, followed by the small WBs (<1 km^2) (*SI Appendix*, Fig. S4 and Table S7). The WB changes vary widely across regions (Fig. 2). For example, the highest absolute increases in area in percentage (13.72%, 16.41%, and

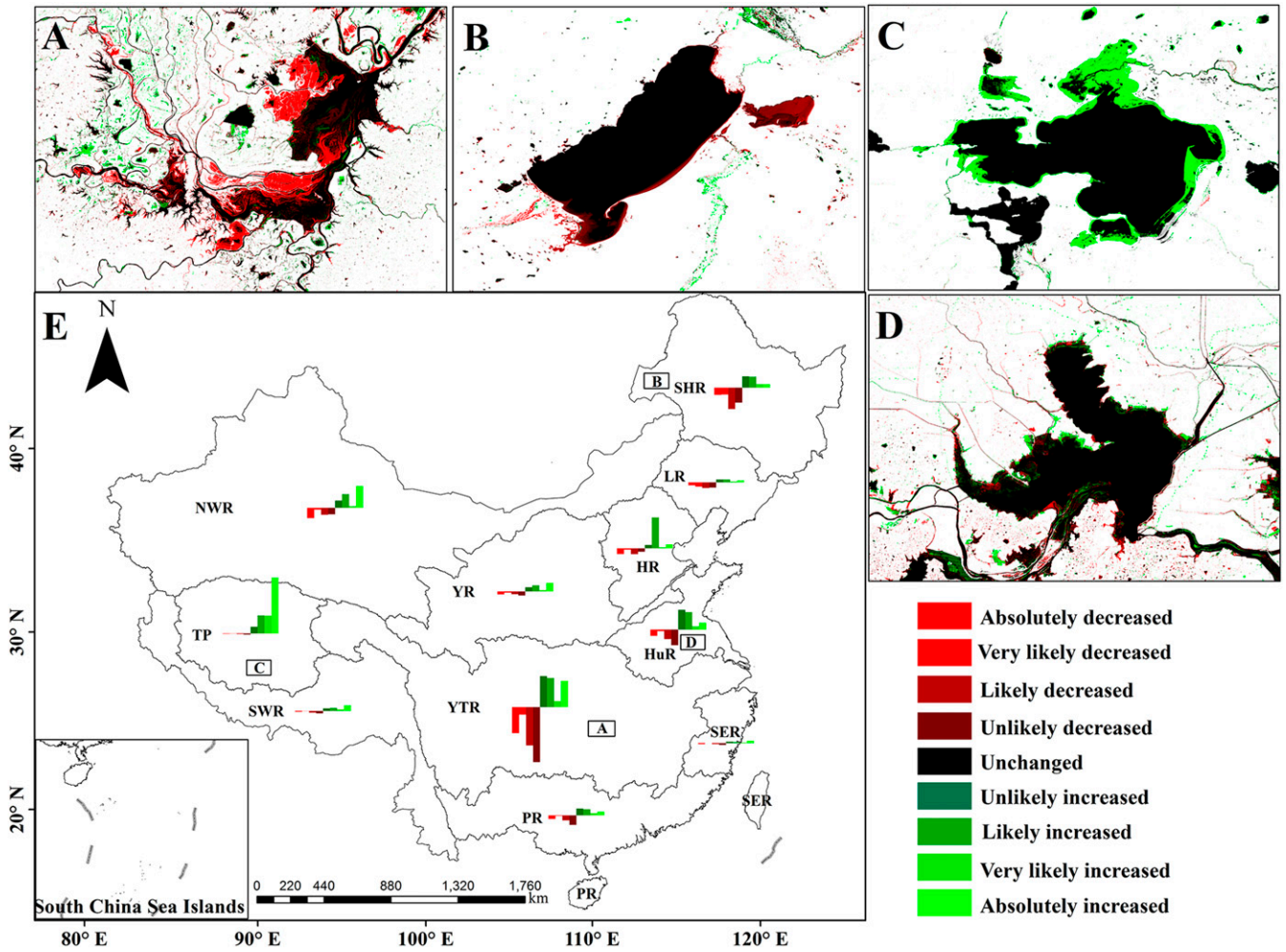

Fig. 2. Regional occurrence changes of WBs at various confidence levels. Subsets of 4 selected cases show WB changes. (*A*) Dongting lake in the YTR, centered at 112.8° E, 29.1°N. (*B*) Hulun lake in the SHR, centered at 117.5°E, 48.9°N. (*C*) Seling Co lake in the TP, centered at 89.1°E, 31.8°N. (*D*) Hongze lake in the HuR, centered at 118.6°E, 33.2°N. (*E*) Epochal changes in different regions.

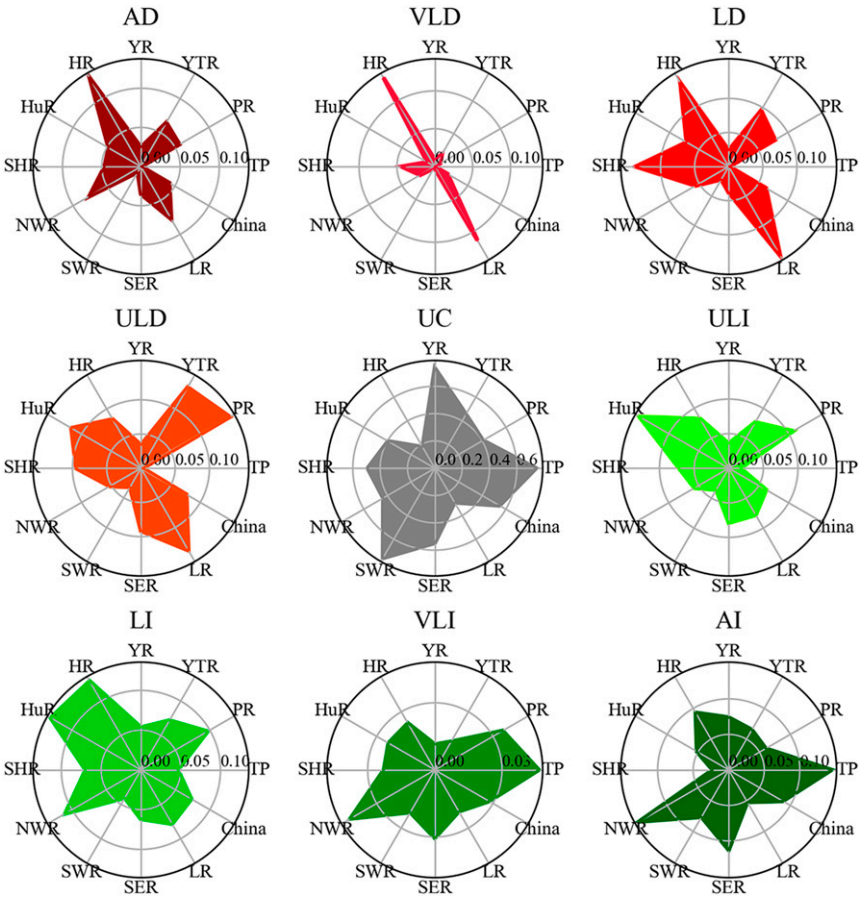

Fig. 3. Epochal changes of water bodies in China and regions at various confidence levels. Changes are classified as Absolutely Decreased (AD), Very Likely Decreased (VLD), Likely Decreased (LD), Unlikely Decreased (ULD), Unchanged (UC), Unlikely Increased (ULI), Likely Increased (LI), Very Likely Increased (VLI), and Absolutely Increased (AI).

9.69%) are found in the TP, Northwest River basins (NWR), and Southeast River basins (SER), respectively. The region that changed the most was the Hai River basin (HR) since only 11.74% of WBs remained unchanged, and the most stable region is the Southwest River basin (SWR) with 75.99% persistently covered by water. The largest absolute decreases in WB occurrence in percentage are found in the HR, SHR, and YTR account for 14.26%, 7.83%, and 5.47% of their total WB areas, respectively.

Our analysis shows a net gain (absolute change) of 3,843 km^2 in WB between the 2 epochs. Although some previous studies have quantified an increase (34, 35), decrease (22, 24), or net change of the WB area in China, they are not comparable to our estimate because of the differences in time span and definitions of change. Our change, following Pekel et al. (19), is defined as the difference between 2 epochs or periods while it is defined as the difference between 2 time points or years in other studies. Consequently, our estimate of change likely represents permanent changes whereas the estimate using other definitions would be more likely influenced by the interannual variability in the climate and hydrologic conditions. Starting with a dry year and ending with a wet year would contain false signals of WB increase; for example, when using the second definition.

Driving Forces of WB Changes

WB changes across the country show great divergent trends (Fig. 3), which were most likely driven by multiple compounding drivers such as climate change and direct human land use change activities (22, 35) (Table 1). Climate change has been shown to have a major impact on WB changes, particularly in the TP and NWR regions. Because of the TP's high elevation and sparse population, its WBs are predominantly influenced by climate change. Despite a decline in only some areas, the widespread increase of WBs in the TP is primarily entailed by multiple climate-related factors, including the precipitation, temperature, glacier, and permafrost (36, 37). On the one hand, the climate change in the TP is prevalently accelerating, as the mean annual precipitation has increased 20 mm and mean annual air temperature has warmed 1.6 °C from 2000 to 2014 (26), resulting in the expansion of existing WBs and formation of new WBs by melting glacier and snow in high mountains. On the other hand, permafrost degradation and WB shrinkage have also been observed in some localized areas with drier climate and reduced precipitation, especially in the area between the Himalayas and Tanggula Mountains and north of the Hengduan Mountains (26). Similarly, increasing WBs are observed in the less populated mountainous areas in the NWR region, caused by glacier melting and an increase in precipitation (38). The dry climate and drought events in the arid regions (e.g., Inner Mongolia Plateau and part of the Xinjiang Uygur Autonomous Region) have also contributed to WB shrinkage (35, 39).

Land use change activities have contributed to the expansion and/or contraction, disappearance, and emergence of WBs at different locations throughout the country. For example, dam constructions can substantially change WB in the upstream and downstream regions (34, 40). Using the YTR basin as an example, both the numbers and surface areas of the reservoirs in the YTR have increased rapidly during past decades, and the impoundment of the great Three Gorges Dam alone formed a

Table 1. Summary of main driving forces in different regions

Region	Main driving forces	References
TP	variations of precipitation; warming-induced glacier-melting and permafrost degradation	Mao et al., 2018b, Zhang et al., 2017a
PR	land reclamation; waterbody impoldering; urbanization	Li et al., 2018; Guo et al., 2015
YTR	dam constructions; aquacultural change; land reclamation or impoldering; urban expansion; sand mining and illegal sand dredging	Cai et al., 2016; Xie et al., 2003
YR	intensification of agriculture; intensified groundwater exploitation	Shi et al., 2011; Zhang et al., 2003
HR	rapid urbanization; land reclamation or waterbody impoldering	Yang et al., 2011; Tian et al., 2016
HuR	dam and floodgate construction; land reclamation	Hu et al., 2008; Zhang et al., 2009
SHR	intensification of agriculture; irrigation; wetland draining or restoration	Xie et al., 2018; Ma et al., 2010
NWR	persistent drought; intensification of agriculture (irrigation); mining	Fang et al., 2018; Tao et al., 2015
SWR	variations of precipitation; warming-induced glacier-melting	Wu et al., 2007; Mao et al., 2018b
SER	aquacultural change; land reclamation or waterbody impoldering	Lu et al., 2015; Wu et al., 2018
LR	intensification of agriculture (irrigation); wetland conversion	Xie et al., 2018; Ma et al., 2010

new large reservoir with an area of 1,084 km^2 in 2003 when it was put into full operation (41). Intensification of agriculture also brings heavy pressure to WBs (40, 42). For example, the northeast region has experienced a rapid increase (319.0%) in irrigated cropland area in the past 3 decades (22, 43). Aquacultural change affects the dynamics of WBs in China, particularly in the east, south central, and southeast regions where water resources and climate are suitable for aquaculture (33). Land reclamation, or WB impoldering (i.e., conversion of WBs into other land uses), has resulted in the loss or shrinking of WBs (38, 41). Many natural wetlands and WBs have been drained and transformed into croplands, grasslands, and woodlands (22, 43), resulting in the loss of about 50,360 km^2 or 14.18% of the wetlands across the country from 1990 to 2000 alone. Many small WBs are infilled in the process of urban expansion (41). Wuhan, the capital city of Hubei province and once known as the city with thousands of lakes, has lost about 70% of its lakes to reclamation and development between 1994 and 2014 (44). Various policies are being put forward by Chinese government to promote wetland conservation and restoration in recent years (45). After joining the Ramsar Convention in 1992, the Chinese government has implemented the National Wetland Conservation Plan, trying to prevent natural wetlands from further loss and degradation (43). The government had funded more than 200 pilot programs with 20.7 billion US$ from 1990 to 2007 to restore degraded wetlands and create new ones to make amends for lost wetlands (46).

Assessing the dynamics of WBs over large regions has been a major challenge because of the constraints in data availability, heterogeneity of environments, and the complexity of driving forces (8). Many studies have mapped WBs with multispectral and hyperspectral images and built databases comprising locations, sizes, and distributions of WBs over large regions (17, 47). However, these studies often suffer from 2 weaknesses. First, they usually do not have enough data points in time to capture the temporal changes of WBs. For instance, results are often generated from subsamples of available remote sensing data at 5-y or longer time intervals (48), representing only snapshots of WB conditions in the sampled years. As a result, the overall dynamics and size dimensions of the WBs, particularly the intermittent WBs, are not well represented (17, 18). Second, the minimal detectable WB size, defined by the resolution of remotely sensed data (e.g., Terra/Aqua MODIS), is usually not fine enough to detect the small WBs that are biologically more active than the large ones (49). Our study shows that the use of dense long-term satellite data at appropriate resolution has the potential to overcome some of the difficulties and reveal unprecedented distributional details and dynamics of WBs over large areas. This capability is essential for validating the relevant theories, such as the power scaling relationship between size and abundance and for adequately scaling many hydrological and biogeochemical processes (e.g., the carbon cycle) from individual aquatic systems to regional and global scales (50). It is also important to map the details of WB changes and understand their causes and consequences to improve water-resource management and planning.

Materials and Methods

Study Area and Region Boundaries. China (73°33′-135°2′E and 3°52′-53°33′E) is our study area (Fig. 1*A*). To investigate the regional differences of WBs, we delineated China into 11 large regions, primarily following the region boundaries from HydroSHEDS (http://www.hydrosheds.org, last accessed in 2018) (51) and National Lake-Watershed Science Data Center (http://lake.geodata.cn). The abbreviations of the regions are listed in *SI Appendix*, Table S3.

Extraction of Lakes, Ponds, and Impoundments. The Global Surface Water Dataset (GSWD), published by the European Commission's Joint Research Centre, was the basis for our study (https://global-surface-water.appspot.com, last accessed on December 12 in 2018). GSWD was generated using 3,066,102 (1,823 terabytes of data) scenes from Landsat 5, 7, and 8 acquired between 16 March 1984 and 31 December 2015 (19). To address the challenges in separating water from other surfaces on the global scale over multiple decades, expert systems, visual analytics, and evidential reasoning techniques were exploited. Details about the implementations of these techniques can be found in Pekel et al. (19). The resultant maps constitute the long-term water history that show the "when and where" of the water presence during the observation period. At the same time, the Water Occurrence, Occurrence Change Intensity, Seasonality, Recurrence, Transitions, MWE are also shown in the dataset. The accuracy of the water maps was assessed by the developers of GSWD in term of errors of omission and commission at the pixel scale (i.e., 30 m) using a total of 40,124 control points distributed both geographically (globally), temporally (across the 32 y). Overall, errors of commission were less than 1% and omission less than 5%.

The data layer showing the MWE (all locations ever mapped as water) during the 32 y was used to extract the locations and maximum extents of WBs in our study. GSWD contains 3 types of waters: artificial paddy fields, rivers, and others (i.e., lakes, ponds, wetlands, and impoundments). As our goal was to investigate the characteristics and dynamics of lakes, ponds, wetlands, and impoundments, rivers and rice paddy fields were removed from the MWE map using the HydroSHEDS data through overlay operation in ArcGIS v10.2 (ESRI) and manually corrected by visual inspection against Google Earth high-resolution images. Consequently, the temporal changes of rivers and streams were also effectively excluded from this analysis (*SI Appendix*, Text S1). Paddy fields in the MWE were removed by referring to the Global Land Cover dataset (GLCD) (http://www.globallandcover.com, last accessed in 2018).

WB Change between 2 Epochs. GSWD provides water occurrence change intensity (OCI) between 2 epochs (i.e., 1984 to 1999, and 2000 to 2015), which was derived from water occurrence difference between homologous pairs of months (19). Specifically, the water occurrence difference for each homologous pair of months between epochs was calculated, and then differences between all homologous pairs of months were averaged to create the surface water OCI map between the epochs. The OCI map shows where surface water

occurrence increased, decreased, or remained invariant, providing a summary of the location and persistence of water in space between the 2 epochs. The OCI map represents the degree of change as a percentage with values ranging from −100 to 100%; positive values indicate increase in occurrence while negative ones show loss of occurrence, and 0% suggests no change in occurrence between the epochs. To summarize the results, OCI values were grouped into several classes: 75 to 99% (high OCI), 25 to 74% (medium OCI), 1 to 24% (low OCI), 0% (unchanged), and 100% (absolutely changed). In essence, these OCI classes effectively represent the probabilities or likelihoods of conversion from nonwater to water (positive OCI) or from water to other surfaces (negative OCI) between 2 epochs, which resulted in 9 generalized probability classes of conversion between water and other land covers: absolutely decreased (OCI = −100%), very likely decreased (OCI = −99% to −75%), likely decreased (OCI = −74 to −25%), unlikely decreased (OCI = −24 to −1%), unchanged (OCI = 0%), unlikely increased (OCI = 1 to 24%), likely increased (OCI = 25 to 74%), very likely increased (OCI = 75 to 99%), and absolutely increased (OCI = 100%).

The minimum water surface area detectable is the pixel size of Landsat (0.0009 km^2). To facilitate comparison with other studies, whenever necessary, WBs were classified into 3 categories of small (<1 km^2), medium (1 to 100 km^2), and large (>100 km^2) following the classification scheme of most previous studies (35, 39). All data processing and analysis were performed using ARCGIS 10.2 (ESRI) and Python 3.6.

Data Availability. All data used in support of this manuscript are available in Figshare (https://figshare.com/s/9e931d6db628e3f96689; DOI: 10.6084/m9.figshare.9959516).

ACKNOWLEDGMENTS. The project was supported by the Ecology Program with funding from Central South University of Forestry and Technology (CSUFT) and the Bureau of Education, Hunan Province, China, the Scientific Innovation Fund for Post-graduates of CSUFT (CX20190631/CX20192037), and National Natural Science Foundation of China (41971152). Data from European Commission Joint Research Centre and HydroSHEDS are greatly appreciated. We also thank the anonymous reviewers for their valuable comments.

1. R. K. Pachauri *et al*. *Climate Change 2014: Synthesis Report. Contribution of Working Groups I, II and III to the Fifth Assessment Report of the Intergovernmental Panel on Climate Change* (IPCC, 2014).
2. S. Baller, S. Dutta, B. Lanvin, *Global Information Technology Report 2016* (Ouranos Geneva, 2016).
3. Z. Zou *et al*., Divergent trends of open-surface water body area in the contiguous United States from 1984 to 2016. *Proc. Natl. Acad. Sci. U.S.A.* **115**, 3810–3815 (2018).
4. R. I. Woolway, C. J. Merchant, Worldwide alteration of lake mixing regimes in response to climate change. *Nat. Geosci.* **12**, 271–276 (2019).
5. S. Piao *et al*., The impacts of climate change on water resources and agriculture in China. *Nature* **467**, 43–51 (2010).
6. T. Oki, S. Kanae, Global hydrological cycles and world water resources. *Science* **313**, 1068–1072 (2006).
7. B. Lehner, P. Döll, Development and validation of a global database of lakes, reservoirs and wetlands. *J. Hydrol. (Amst.)* **296**, 1–22 (2004).
8. C. Verpoorter, T. Kutser, D. A. Seekell, L. J. Tranvik, A global inventory of lakes based on high-resolution satellite imagery. *Geophys. Res. Lett.* **41**, 6396–6402 (2014).
9. E. Hotchkiss *et al*., Sources of and processes controlling CO_2 emissions change with the size of streams and rivers. *Nat. Geosci.* **8**, 696–699 (2015).
10. G. H. Allen, T. M. Pavelsky, Global extent of rivers and streams. *Science* **361**, 585–588 (2018).
11. M. A. Holgerson, P. A. Raymond, Large contribution to inland water CO_2 and CH_4 emissions from very small ponds. *Nat. Geosci.* **9**, 222 (2016).
12. B. B. Mandelbrot, *The Fractal Geometry of Nature* (WH freeman, New York, 1982).
13. D. A. Seekell, M. L. Pace, L. J. Tranvik, C. Verpoorter, A fractal-based approach to lake size-distributions. *Geophys. Res. Lett.* **40**, 517–521 (2013).
14. M. K. Steele, J. B. Heffernan, Land use and topography bend and break fractal rules of water body size-distributions. *Limnol. Oceanogr. Lett.* **2**, 71–80 (2017).
15. P. V. Mosquera, H. Hampel, R. F. Vázquez, M. Alonso, J. Catalan, Abundance and morphometry changes across the high-mountain lake-size gradient in the tropical Andes of Southern Ecuador. *Water Resour. Res.* **53**, 7269–7280 (2017).
16. D. A. Seekell, M. L. Pace, Does the Pareto distribution adequately describe the size-distribution of lakes? *Limnol. Oceanogr.* **56**, 350–356 (2011).
17. M. L. Messager, B. Lehner, G. Grill, I. Nedeva, O. Schmitt, Estimating the volume and age of water stored in global lakes using a geo-statistical approach. *Nat. Commun.* **7**, 13603 (2016).
18. Y. Sheng *et al*., Representative lake water extent mapping at continental scales using multi-temporal Landsat-8 imagery. *Remote Sens. Environ.* **185**, 129–141 (2016).
19. J.-F. Pekel, A. Cottam, N. Gorelick, A. S. Belward, High-resolution mapping of global surface water and its long-term changes. *Nature* **540**, 418–422 (2016).
20. S. K. Hamilton, J. M. Melack, M. F. Goodchild, W. Lewis, "Estimation of the fractal dimension of terrain from lake size distributions" in *Lowland Floodplain Rivers: Geomorphological Perspectives*, P. A. Carling, G. E. Petts, Eds. (Wiley, 1992), pp. 145–163.
21. M. E. Newman, Power laws, Pareto distributions and Zipf's law. *Contemp. Phys.* **46**, 323–351 (2005).
22. R. Ma *et al*., A half-century of changes in China's lakes: Global warming or human influence? *Geophys. Res. Lett.* **37**, L24106 (2010).
23. R. Ma *et al*., China's lakes at present: Number, area and spatial distribution. *Sci. China Earth Sci.* **54**, 283–289 (2011).
24. X. Yang, X. Lu, Drastic change in China's lakes and reservoirs over the past decades. *Sci. Rep.* **4**, 6041 (2014).
25. X. Yang, X. X. Lu, Delineation of lakes and reservoirs in large river basins: An example of the Yangtze River Basin, China. *Geomorphology* **190**, 92–102 (2013).
26. D. Mao *et al*., Impacts of climate change on Tibetan Lakes: Patterns and processes. *Remote Sens.* **10**, 358 (2018).
27. W. Wan *et al*., Monitoring lake changes of Qinghai-Tibetan Plateau over the past 30 years using satellite remote sensing data. *Chin. Sci. Bull.* **59**, 1021–1035 (2014).
28. S. Lu *et al*., Lake water surface mapping in the Tibetan Plateau using the MODIS MOD09Q1 product. *Remote Sens. Lett.* **8**, 224–233 (2016).
29. F. Aires *et al*., Comparison of visible and multi-satellite global inundation datasets at high-spatial resolution. *Remote Sens. Environ.* **216**, 427–441 (2018).
30. C. P. McDonald, J. A. Rover, E. G. Stets, R. G. Striegl, The regional abundance and size distribution of lakes and reservoirs in the United States and implications for estimates of global lake extent. *Limnol. Oceanogr.* **57**, 597–606 (2012).
31. C. Hohenegger, B. Alali, K. R. Steffen, D. K. Perovich, K. M. Golden, Transition in the fractal geometry of Arctic melt ponds. *Cryosphere* **6**, 1157–1162 (2012).
32. J. Gao, Z.-g. Xia, Fractals in physical geography. *Prog. Phys. Geogr.* **20**, 178–191 (1996).
33. P. Jia, W. Zhang, Q. Liu, Lake fisheries in China: Challenges and opportunities. *Fish. Res.* **140**, 66–72 (2013).
34. C. Xie, X. Huang, J. Li, Assessing China's Lake changes and associated driving forces during 1985–2015. *Photogramm. Eng. Remote Sens.* **84**, 657–666 (2018).
35. G. Zhang *et al*., Regional differences of lake evolution across China during 1960s–2015 and its natural and anthropogenic causes. *Remote Sens. Environ.* **221**, 386–404 (2019).
36. G. Zhang *et al*., Extensive and drastically different alpine lake changes on Asia's high plateaus during the past four decades. *Geophys. Res. Lett.* **44**, 252–260 (2017).
37. G. Zhang, T. Yao, H. Xie, K. Zhang, F. Zhu, Lakes' state and abundance across the Tibetan Plateau. *Chin. Sci. Bull.* **59**, 3010–3021 (2014).
38. L. Fang, S. Tao, J. Zhu, Y. Liu, Impacts of climate change and irrigation on lakes in arid northwest China. *J. Arid Environ.* **154**, 34–39 (2018).
39. S. Tao *et al*., Rapid loss of lakes on the Mongolian Plateau. *Proc. Natl. Acad. Sci. U.S.A.* **112**, 2281–2286 (2015).
40. Y. Zhang, J. Xia, T. Liang, Q. Shao, Impact of water projects on river flow regimes and water quality in Huai River Basin. *Water Resour. Manage.* **24**, 889–908 (2009).
41. X. Cai, L. Feng, X. Hou, X. Chen, Remote sensing of the water storage dynamics of large lakes and reservoirs in the Yangtze River Basin from 2000 to 2014. *Sci. Rep.* **6**, 36405 (2016).
42. W. Yuan *et al*., Opportunistic market-driven regional shifts of cropping practices reduce food production capacity of China. *Earths Futur.* **6**, 634–642 (2018).
43. Z. Wang, J. Wu, M. Madden, D. Mao, China's wetlands: Conservation plans and policy impacts. *Ambio* **41**, 782–786 (2012).
44. X. Bai, P. Shi, Y. Liu, Society: Realizing China's urban dream. *Nature* **509**, 158–160 (2014).
45. S. Zhao, J. Fang, Impact of impoldering and lake restoration on land-cover changes in Dongting Lake area, Central Yangtze. *Ambio* **33**, 311–315 (2004).
46. L. Luo *et al*., Remote sensing and GIS support to identify potential areas for wetland restoration from cropland: A case study in the west songnen plain, Northeast China. *Sustainability* **10**, 2375 (2018).
47. X. Tong *et al*., Estimating water volume variations in Lake Victoria over the past 22 years using multi-mission altimetry and remotely sensed images. *Remote Sens. Environ.* **187**, 400–413 (2016).
48. S.-Y. Wang, J.-S. Liu, T.-B. Ma, Dynamics and changes in spatial patterns of land use in Yellow River Basin, China. *Land Use Policy* **27**, 313–323 (2010).
49. A. Khandelwal *et al*., An approach for global monitoring of surface water extent variations in reservoirs using MODIS data. *Remote Sens. Environ.* **202**, 113–128 (2017).
50. P. A. Raymond *et al*., Global carbon dioxide emissions from inland waters. *Nature* **503**, 355–359 (2013).
51. B. Lehner, K. Verdin, A. Jarvis, New global hydrography derived from spaceborne elevation data. *Eos* **89**, 93–94 (2008).